Available online at www.sciencedirect.com

ScienceDirect

Underground Space 26 (2026) 305–320

www.keaipublishing.com/undsp

Research Paper

Development of surface settlement under the combined effect of foundation pit dewatering and excavation: Insights from experimental modelling

Kai-Fang Yang [a,b,c], Min-Liang Chi [a], Chang-Jie Xu [a,d,*], Chao-Feng Zeng [e], Lu-Jv Liang [b,f], Zhi Ding [a,b], Ya-Shi Qiu [a]

[a] College of Civil Engineering and Architecture, Zhejiang University, Hangzhou 310058, China
[b] School of Engineering, Hangzhou City University, Hangzhou 310015, China
[c] School of Civil Engineering and Architecture, Zhejiang University of Science and Technology, Hangzhou 310012, China
[d] School of Civil Engineering and Architecture, East China Jiaotong University, Nanchang 330013, China
[e] Hunan Provincial Key Laboratory of Geotechnical Engineering for Stability Control and Health Monitoring, School of Civil Engineering, Hunan University of Science and Technology, Xiangtan 411201, China
[f] Key Laboratory of Safe Construction and Intelligent Maintenance for Urban Shield Tunnels of Zhejiang Province, Hangzhou 310015, China

Received 29 November 2024; received in revised form 27 June 2025; accepted 10 July 2025
Available online 7 November 2025

Abstract

To investigate surface settlement under the combined effect of foundation pit dewatering and excavation, a series of experiments was conducted using a scaled model of a deep foundation pit at a metro station. During experimental simulations of the dry excavation and dewatering processes, data were collected on surface settlement, water heads outside the pit, and deflection of the diaphragm wall. The characteristics of surface settlement were compared and analyzed under different conditions with a focus on the development of surface settlement during dewatering and excavation at key locations outside the pit. The combined effect of dewatering and excavation was found to increase surface settlement outside the pit and expand its area of influence. The insertion ratio of the diaphragm wall (n) significantly affected surface settlement; as the insertion ratio increased, surface settlement, along with its area of influence, decreased. For $n < 1.25$, the area beyond twice the excavation depth was considered a minor area of settlement influence. In contrast, for $n \geq 1.25$, this area wasn't classified as a minor area of settlement influence. As excavation depth increased, the surface settlement pattern outside the pit transitioned from triangle-type to groove-type, groove-type settlement occurred when $A_s \geq 1.6A_c$, whereas triangle-type settlement occurred under other conditions (A_s represents the area of the deep inward part of the convex deformation of the diaphragm wall; A_c refers to the cantilever part of the diaphragm wall). This study provides insights into the development of surface settlement during dewatering and excavation and serves as a valuable reference for innovations in sustainable and resilient underground design.

Keywords: Foundation pit dewatering; Deep excavation; Sustainability; Surface settlement; Laboratory test; Insertion ratio

1 Introduction

Recent urbanization has intensified the development of underground spaces such as subway stations and building basements. Consequently, increasingly large and deep foundation pits are being designed. However, these deep foundation pit projects are associated with new challenges (Tan et al., 2018; Xu et al., 2021; Pujades-Garnes et al.,

* Corresponding author at: College of Civil Engineering and Architecture, Zhejiang University, Hangzhou 310058, China.
E-mail address: xucj@zju.edu.cn (C.-J. Xu).
Peer review under the responsibility of Tongji University.

https://doi.org/10.1016/j.undsp.2025.07.003

2024). In areas with abundant groundwater resources, particularly water-rich sand layers, high groundwater heads often present challenges when excavating foundation pits (Wang et al., 2019; Yang et al., 2022; Ping et al., 2024). As the depth of excavation increases, dewatering and excavation can lead to uneven surface settlement outside the pit, resulting in engineering accidents (M. Li et al., 2020; Zeng et al., 2021; Yang et al., 2023; Ge et al., 2024). Therefore, under the combined effect of foundation pit dewatering and excavation, the excavation depth, groundwater drawdown, and the form of the surrounding structure are key factors influencing surface settlement. To ensure the safety of foundation pit projects and to protect the surrounding buildings, accurately estimating the ground settlement caused by dewatering and excavation is crucial (Serrano-Juan et al., 2018; Zeng et al., 2024; Zheng et al., 2024).

The unloading of soil from a foundation pit can cause the diaphragm wall to move inward (Xu et al., 2021; Fan et al., 2024; Ding et al., 2024; Abbas et al., 2023). This movement can cause both vertical and lateral shifts in the soil layers outside the foundation pit, resulting in uneven surface settlement outside the pit (Li et al., 2022; Dong et al., 2023; Guan et al., 2024). Researchers have proposed various empirical (Clough & O'Rourke, 1990; Ou et al., 1993; Hsieh & Ou, 1998; Wang et al., 2023; Chen et al., 2018) and analytical (Fan et al., 2021; Abbas et al., 2023; Li et al., 2024; Tang et al., 2024) formulas for predicting the stress and deformation of the diaphragm wall due to dewatering and excavation, along with the resulting settlement of the surface outside the pit and the types of settlement. Researchers have also investigated the lateral displacement of the diaphragm wall and the surface settlement caused by excavation through numerical methods (Li et al., 2022; Dong et al., 2023; Cui et al., 2023; Wang et al., 2023), model tests (Dong et al., 2023; Ge et al., 2024; Fan et al., 2024), field tests (Cui et al., 2023; Yang et al., 2023; Ge et al., 2024), and machine learning techniques (Zhang et al., 2024).

However, the studies mentioned above primarily focus on the effects of foundation pit excavation on surface settlement outside the pit. When the diaphragm wall does not fully isolate the aquifer, dewatering can lower the groundwater level outside the pit and cause the diaphragm wall to shift sideways (Zhang et al., 2017; Luo et al., 2018; Wu et al., 2020; Zeng et al., 2022; Yang et al., 2022). Both effects can lead to uneven surface settlement, deformation of structures, and even structural failure (M. Li et al., 2020; Zeng et al., 2022; Xue et al., 2024). Many researchers have studied groundwater level and surface settlement caused by foundation pit dewatering through theoretical analysis (Luo et al., 2018; J. Li et al., 2020; Wu et al., 2020; Yang et al., 2022), numerical simulation (Zhang et al., 2017; Wang et al., 2019; M. Li et al., 2020; Xue et al., 2024; Ping et al., 2024), model tests (Pujades & Jurado, 2021; Zeng et al., 2021; Wang et al., 2022), and field tests (Serrano-Juan et al., 2017; W. Zhang et al., 2018; Tan et al., 2018; Zeng et al., 2024). However, most studies have concentrated on surface settlement caused by pre-dewatering, while the effect of dewatering during the excavation process is often neglected. Although some research has analyzed how the interaction between excavation and dewatering affects the ground surface (Hsi & Small, 1992; Y. Zhang et al., 2018; Park et al., 2020), the combined effect of pit dewatering and excavation unloading on surface settlement remains unclear.

In summary, few studies have analyzed surface settlement under the combined influence of both pit dewatering and excavation. In this paper, we investigate surface settlement resulting from the combined effect of dewatering and excavation by conducting a series of laboratory-scale experiments using a model of a foundation pit based on a metro station in Nanchang, Jiangxi Province, China. We compared and analyzed the characteristics of surface settlement under various conditions and discussed the patterns of settlement during dewatering and excavation at key locations outside the pit. Additionally, we thoroughly investigated the relationship between the type of settlement pattern and the lateral displacement shape of the diaphragm wall.

2 Experimental system

2.1 Engineering background

The experimental model was based on a metro station on Nanchang Metro Line No. 4 in Jiangxi Province. Figure 1 illustrates the layout of the foundation pit and simulation area. The station has a total length of 238 m and a standard width of 22.7 m. The excavation depth for the standard section is approximately 16 m, while the excavation depth for the end well section is approximately 17.2 m. The design of the retaining structure incorporates diaphragm walls coupled with an internal support system. The diaphragm wall consists of C35 reinforced concrete, with a thickness of 800 mm and a depth of approximately 28 m. The cross-sectional dimensions of the first support are 800 mm × 1000 mm, with a spacing of 12.0 m. The steel pipe supports have diameters of 609 mm and wall thicknesses of 16 mm, with a horizontal spacing of 3.0 m.

Nanchang has a subtropical monsoon climate with abundant rainfall and widespread lakes and groundwater. The foundation pit is mainly affected by the phreatic aquifer, which is located in silty clay, fine sand, and coarse sand. Because sandy soil has a large gravitational water release characteristic, excavation may cause landslide, sand flow, and other adverse phenomena if no measures are taken to decrease the moisture content of the soil layer (Yang et al., 2022). Geologic exploration revealed that the excavation area of the station extends into the Quaternary sand aquifer, which has a permeability coefficient of 30 m/d, indicating high permeability.

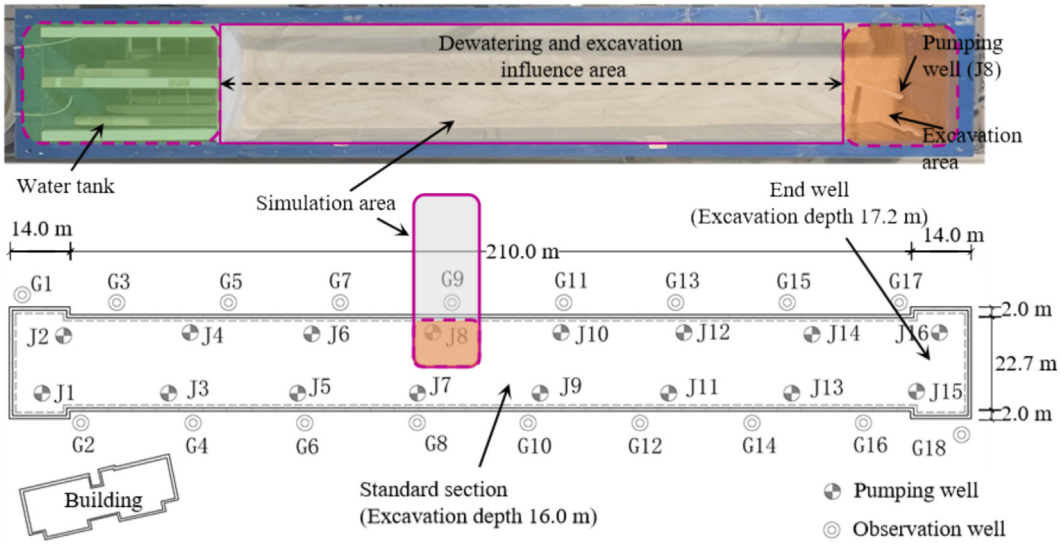

Fig. 1. Plan view showing the simulated area of the subway station foundation pit.

The water level is located from approximately 4.1–7.0 m below the ground surface. A total of 16 pumping wells and 18 observation wells have been installed inside and outside the foundation pit. One pumping well and two observation wells are used to conduct a single-well pumping test on a partially penetrating well in a phreatic aquifer. Additionally, this model experiment is also based on the soil properties of the pumping test site, which are used for conducting the study.

2.2 Experimental design

This subway station has a long and narrow foundation pit. Therefore, in this study, we focused exclusively on the simulation area depicted in Fig. 1, specifically the region where dewatering well J8 and observation well G9 are located. It is important to note that this model does not perfectly replicate the actual pit; thus, a strict similarity ratio was not implemented for the soil around the pit. The simulated area represents the middle section of the foundation pit, which is not influenced by corner effects and experiences plane strain conditions, and the model experiment simultaneously simulates the length direction of the simulated area. Consequently, experiments using this model can be considered quasi-three-dimensional tests, which can more accurately replicate the development of surface settlement resulting from the combined effect of foundation pit dewatering and excavation.

Figure 2 shows images of the model used in the experiments. Since the experiments were conducted under 1*g* scale conditions, it was challenging to satisfy all physical and mechanical similarity requirements. The primary objective was to achieve an accurate similarity for the diaphragm wall; specifically, the size and stiffness of the diaphragm wall were controlled to achieve the desired similarity ratio. Based on laboratory conditions and existing reports (Zeng et al., 2021), the similarity ratio was set to 1:40.

2.3 Experimental box size

As shown in Fig. 3, the experimental model had dimensions of 260 cm × 60 cm × 120 cm (length × width × height). The model was a steel rectangular box without a cover, featuring a transparent tempered glass observation window along its length. A T-beam was integrated into the middle of the model box to prevent deformation. During the test, the observation window on the side wall of the model box did not exhibit any lateral deformation. Based on the findings of Xu et al. (2019) in a similar dewatering test conducted in sand, both the dewatering influence radius and the excavation influence radius were set to more than four times the maximum excavation depth to accurately reflect the effects of these radii on the results. The recharge water tank measured 50 cm in length, the soil area stretched over 180 cm, and the excavation area was 30 cm in length.

2.4 Excavation area

2.4.1 Retaining structure: Support and diaphragm wall

The similarity ratio for the scale model used in this study was 1:40, and the spacing between the reinforced concrete supports was 12 m. Based on this ratio, the calculated support spacing should be 30 cm. Because the long side of the simulated area for foundation pit excavation was 60 cm, a support was placed at the center of this long side. According to the cross-sectional dimensions of the actual engineering support and existing studies (Fan et al., 2024), polyvinyl chloride (PVC) pipes were selected as the support material. These pipes had an elastic modulus of 3.5×10^3 MPa and

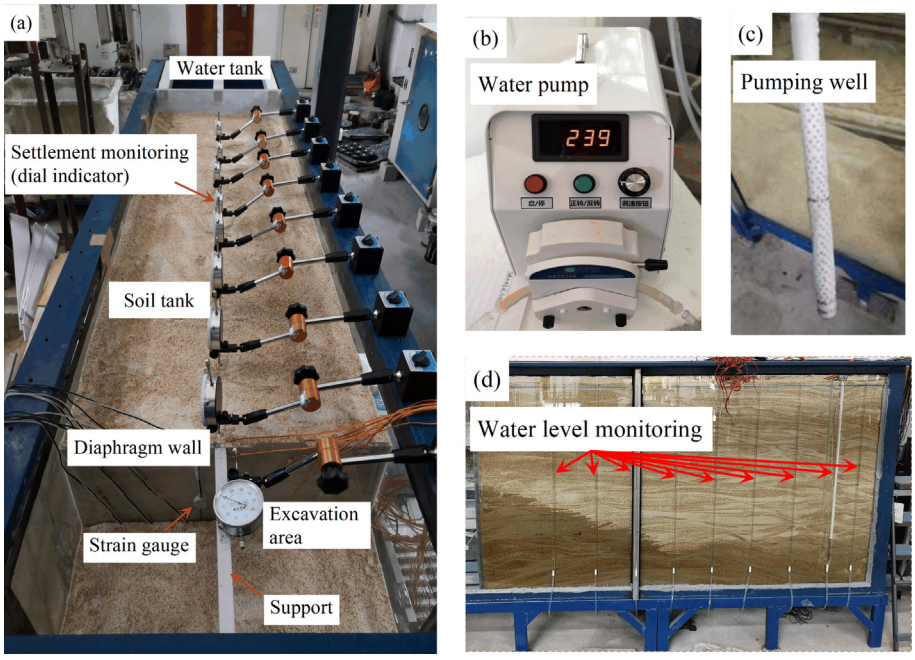

Fig. 2. Images of the model used for dewatering excavation tests. (a) Settlement monitoring, (b) water pump, (c) pumping well, and (d) water level monitoring.

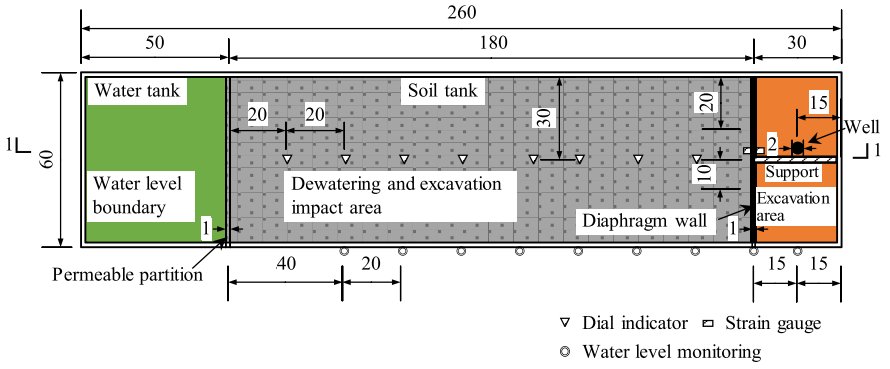

(a)

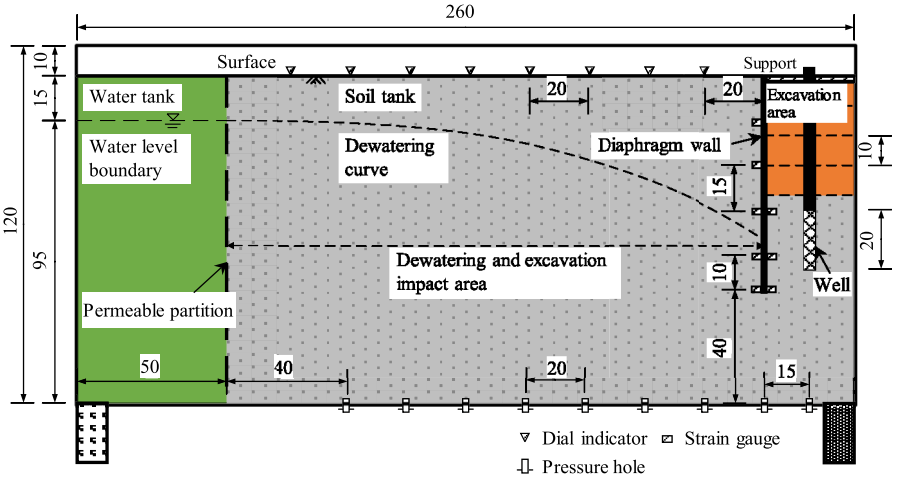

(b)

Fig. 3. Schematic diagram of the dewatering excavation test device. (a) Plan view, and (b) sectional view 1-1. (Unit: cm)

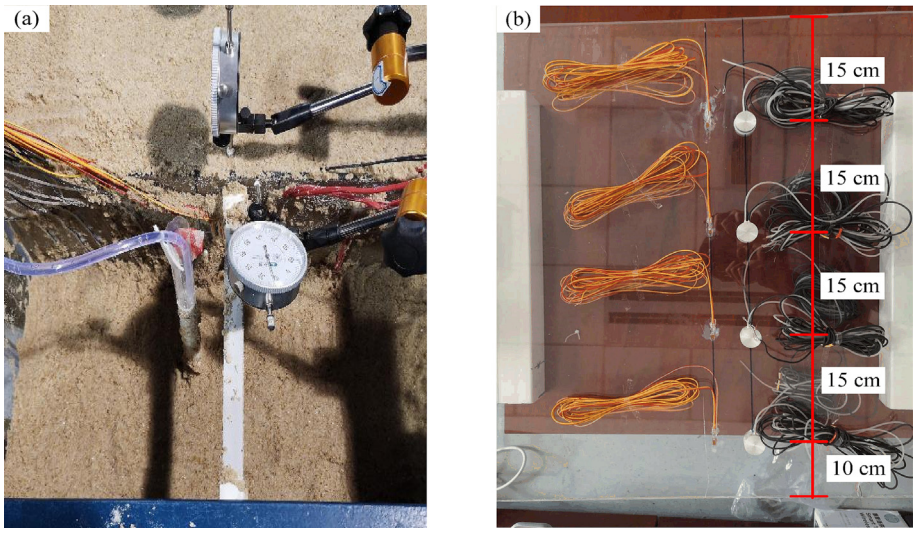

Fig. 4. Images of the retaining structure system. (a) Support, and (b) diaphragm wall.

a Poisson's ratio of 0.38. The designed cross-sectional dimensions of the PVC support pipe were 20 mm × 20 mm. The support layout is illustrated in Fig. 4(a).

Based on Zeng et al. (2023), an organic glass plate was chosen as the diaphragm wall material. The diaphragm wall was designed according to the principle of equivalent similarity in bending stiffness. The thickness of the organic glass plate used for the diaphragm wall was determined as follows:

$$d_m = \frac{d_p}{n}\left(\frac{1-v_m^2}{1-v_p^2}\cdot\frac{E_p}{NE_m}\right)^{\frac{1}{3}}, \quad (1)$$

where E_m is the elastic modulus of the organic glass plate; E_p is the elastic modulus of the underground diaphragm wall; d_m is the thickness of the organic glass plate; d_p is the thickness of the underground diaphragm wall; v_m is the Poisson's ratio of the organic glass plate; v_p is the Poisson's ratio of the underground diaphragm wall; and N is the similarity ratio (1:40).

In the actual engineering project, the diaphragm thickness is 800 mm, and its length is 28 m. The elastic modulus of reinforced concrete is 35 GPa, with a Poisson's ratio of 0.167. In this test, the diaphragm wall was simulated using organic glass, which has an elastic modulus of 3.37 GPa and a Poisson's ratio of 0.25. Substituting these parameters into Eq. (1), the calculated thickness of the organic glass plate was 12 mm with a depth of 70 cm, as shown in Fig. 4(b).

2.4.2 Pumping system

As illustrated in Fig. 2(b), an SR400 box-type peristaltic pump was used for foundation pit dewatering with a maximum flow rate of 1.03 L/min (determined based on calibration experiments). As shown in Fig. 2(c), a PVC pipe with an outer diameter of 20 mm and an inner diameter of 16 mm was used to simulate dewatering. The length of the well pipe was 65 cm, representing an actual engineering dewatering well length of 26 m scaled down 40 times. The filter section length was 20 cm, equivalent to 8 m in actual engineering length, scaled 40 times. To prevent soil particles from clogging the water inlet holes, a nylon filter cloth with an aperture of 0.125 mm was wrapped around the well pipe for back filtration.

2.5 Soil tank

The tests used ISO standard sand sourced from Pingtan, Fujian with a fill thickness of 110 cm. The particle size distribution curve of the sand is shown in Fig. 5, and the specific granular characteristics were as follows: d_{60} = 0.96 mm; d_{30} = 0.35 mm; d_{10} = 0.13 mm; inhomogeneity coefficient (C_u) = 6.92; and curvature coefficient (C_c) = 1.05. According to ASTM D2487-11 (ASTM, 2011) and Chinese Standard GB/T 50145—2007 (Ministry of Water Resources of the People's Republic of China, 2007), the sand could be considered well graded, and it was classified as medium sand.

After filling the model box with sand, the sand parameters were obtained through conventional geotechnical tests, and the average values of three parallel tests were used. The soil parameters are presented in Table 1. The wet density was measured using the ring knife method. The moisture content was determined using the drying method. The relative density was assessed using the specific gravity bottle method. Porosity was calculated based on the measured wet density, moisture content, and relative density, while the permeability coefficient was obtained using the constant head method. The internal friction angle and effective internal friction angle of the sand were measured through triaxial compression tests. The compression modulus was determined from consolidation tests. The constrained modulus of the soil was calculated from the curve of the void ratio vs. the effective stress (Fig. 6).

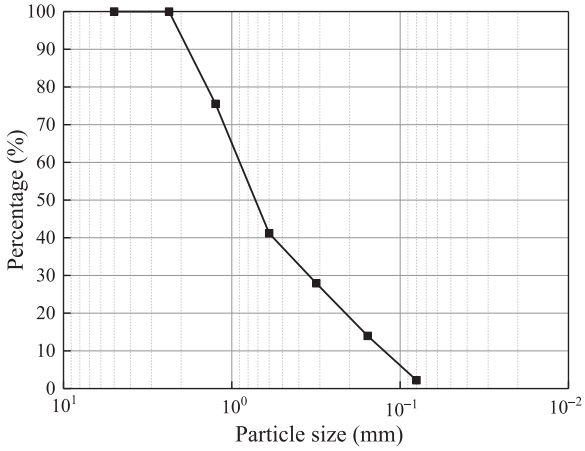

Fig. 5. Particle size distribution of the soil used in the laboratory tests.

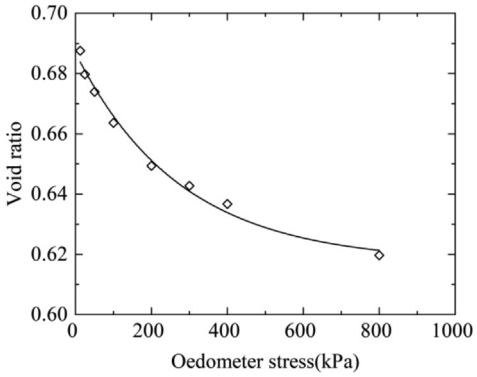

Fig. 6. Relationship between the void ratio and consolidation stress of the soil used in the laboratory test.

2.6 Water tank and water supply system

The water tank, located on the left side of the model box, was separated from the soil tank by a permeable partition. The wall of the water tank was marked with scale lines, and the tank was dynamically replenished using a flow-adjustable pump. The water level in the tank was carefully controlled to maintain a constant head boundary. As shown in Fig. 7, the permeable partition featured evenly distributed perforations across its entire section. The opening rate was 30%, similar to the porosity of the test soil. Filter cloth was attached to both sides to prevent the loss of sand and soil.

2.7 Monitoring device

The monitoring device included a water level monitoring system, dial gauges, and strain gauges. The water level monitoring tubes were connected to the pressure hole at the bottom of the box, with the spacing between the tubes being 20 cm. Dial gauges were installed on the soil surface outside the foundation pit and at the top of the diaphragm wall, with the spacing between the dial gauges being 20 cm. All strain gauges were attached along the centerline of the organic glass diaphragm wall following the spatial arrangement shown in Figs. 2 and 3, with the spacing between the strain gauges being 15 cm.

2.8 Experimental scheme

Many cases have shown that the ratio of the buried depth of the diaphragm wall to the excavation depth generally ranges between 1.6 and 2.2, depending on the soil strata. In this paper, the excavation depth of the model pit was 40 cm; thus, the depths of the diaphragm wall were set to 60, 70, 80, and 90 cm in this study.

As shown in Table 2, model tests were conducted under two conditions: Condition I, the dewatering excavation test, where dewatering and excavation were performed alternately (dewatering followed by excavation); and Condition II, the dry excavation test, which was conducted in four layers.

2.9 Test process

Each test was conducted three times in parallel to eliminate testing errors. Taking the dewatering excavation test of Condition I as an example, the test steps were as follows.

2.9.1 Test preparation

(1) A sealing test was conducted on the model box to ensure that no water seepage occurred.
(2) The permeable partition and diaphragm wall were installed in their designed positions, and the diaphragm wall was sealed with a hard plastic film on both sides.
(3) The box was then filled with sand using an artificial rain method, and the falling distance of the sand was controlled at 500 mm. A specific amount of sand was moved back and forth and laid in the model box at a falling speed of 120 g/s.
(4) When the sand was filled to 3 cm below the ground surface (1 cm below the bottom of the support) on both sides of the diaphragm wall, the support was set up before continuing to fill the model with sand until it reached the height of the diaphragm wall.

Table 1
Physical parameters of the model soil.

Property	ρ (g/cm^3)	w (%)	G_s	e	K (m/d)	E_s (MPa)	φ' (°)
Sand	2.01	29.6	2.67	0.72	18.68	11.67	31.6

Notes: ρ is density; w is water content; G_s is specific gravity; e is void ratio; K is hydraulic conductivity; E_s is constrained modulus; φ' is effective friction angle.

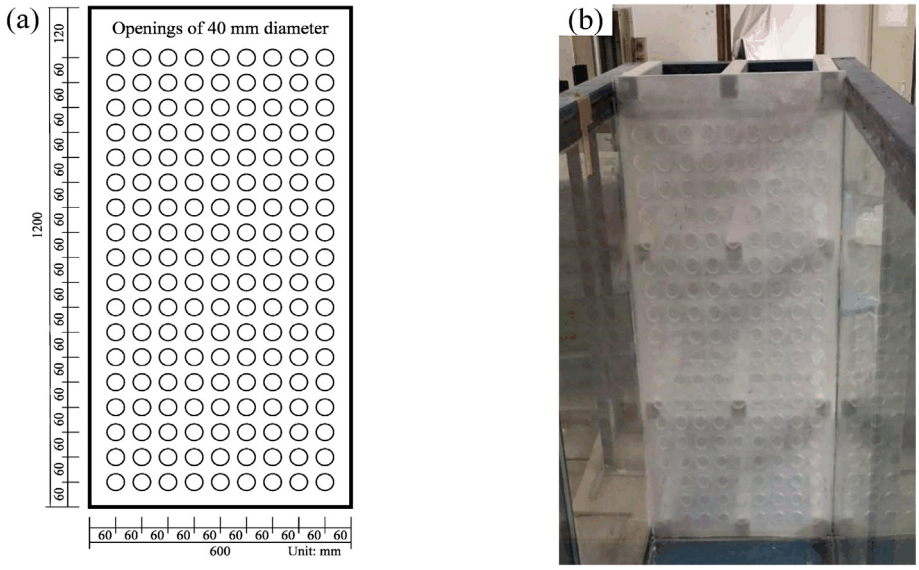

Fig. 7. Filter plate. (a) Diagram of the openings, and (b) image of the plate wrapped in gauze.

Table 2
Conditions of model tests.

Test conditions	n	D (cm)	L (cm)	h (cm)
I: Dewatering excavation	0.50	10, 20, 30, 40	60	−15, −21, −31, −41
	0.75	10, 20, 30, 40	70	−15, −21, −31, −41
	1.00	10, 20, 30, 40	80	−15, −21, −31, −41
	1.25	10, 20, 30, 40	90	−15, −21, −31, −41
II: Dry excavation	0.50	10, 20, 30, 40	60	–
	0.75	10, 20, 30, 40	70	–
	1.00	10, 20, 30, 40	80	–
	1.25	10, 20, 30, 40	90	–

Notes: D is the excavation depth; n is the ratio of the maximum excavation depth D_{max} to the diaphragm wall insertion depth ΔL ($\Delta L = L - D$, where L is the buried depth of the diaphragm wall); and h is the groundwater level, the initial groundwater level was −15 cm, and the groundwater level in the pit was lowered to 1 cm below the excavation depth before the excavation of each layer.

Monitoring devices, including dial gauges, were installed at designated positions and reset to zero for standby.

2.9.2 Water injection and pressurization

(1) The model was connected to the water circulation system, and the speed of the peristaltic pump was adjusted to stabilize the water level in the soil tank at its initial height.
(2) Groundwater flowed through the permeable partition into the soil tank until it reached the initial water level. The water injection was then stopped, allowing the system to stand still.
(3) The head of the pressure measurement tube stabilized, indicating that the soil tank could be considered saturated due to groundwater seepage. This process was allowed to continue for 24 h to complete the consolidation of the soil layer.

2.9.3 Dewatering excavation test

(1) Before excavation, the reading of each pressure-measuring tube was recorded as the initial groundwater level, while the water level in the soil tank was maintained at −15 cm.
(2) The foundation pit was excavated in layers, with each layer having an excavation depth of 10 cm. Manual excavation was performed using a flat shovel with a width of 7.5 cm, which approximated the action of a medium-sized excavator with a bucket width of approximately 3 m.
(3) The data collection system was activated, and the foundation pit was dewatered using a pump. Following the principle of "dewatering first, then excavating", the water level was lowered to 1 cm below the low elevation of each excavation layer and left to stabilize for 30 min (Xu et al., 2019; Zeng et al., 2023).
(4) After stabilization, the reading of each monitoring device was recorded. The soil of that layer was then

excavated to the set height and left to stand for 30 min.

(5) The reading of each monitoring device was again recorded. The above process was repeated until the end of the test.

The dry excavation test followed similar steps, but it did not include the water injection, pressurization, or foundation pit dewatering steps.

3 Experimental model verification

Since this model experiment involves two main processes—dewatering and excavation—it is essential to verify the groundwater drawdown and flow rate with pumping time, as well as the surface settlement outside the pit caused by these processes. Therefore, groundwater drawdown and surface settlement were selected as key parameters for model verification.

3.1 Groundwater drawdown, flow rate, and pumping time

To validate the accuracy of the numerical model, data on groundwater drawdown under four different buried depths of waterproof structures were extracted. These data, illustrated in Fig. 8, demonstrate that the pumping time and flow rate from the numerical model align with the model test results. The groundwater drawdown calculated by the numerical model was slightly lower than that observed in the model test. This discrepancy occurred because the soil layer in the numerical model was considered to be homogeneous, and the permeability coefficient in the model test was larger than that in the numerical model. Despite this experimental error, the trends in groundwater drawdown remained consistent as the buried depth of the waterproof structure increased (Xu et al., 2019; Pujades-Garnes et al., 2024).

3.2 Surface settlement

To verify the reasonableness of the model test data, the surface settlement values outside the pit were normalized

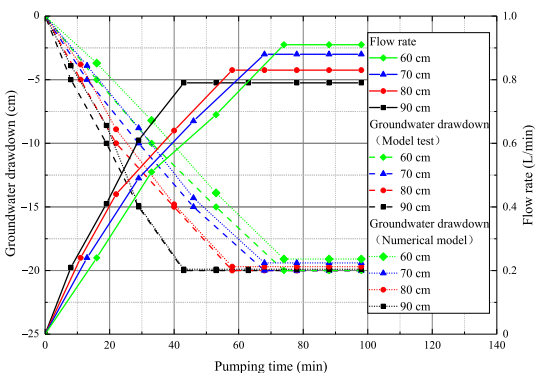

Fig. 8. Changes in groundwater drawdown and flow rate with pumping time.

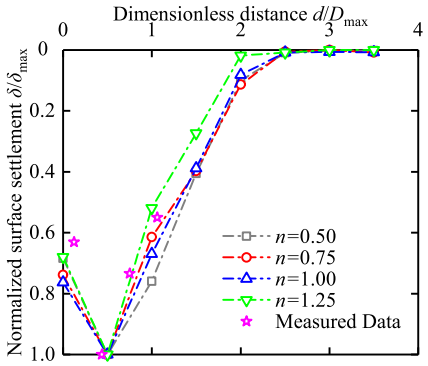

Fig. 9. Comparison of dimensionless surface settlement data between the model test results and measured values.

and compared with the measured values once the excavation reached the bottom of the pit. In this context, D is the depth of excavation, n represents the insertion ratio of the diaphragm wall, δ represents the surface settlement at any point behind the wall, δ_{max} is the maximum surface settlement behind the wall, d is the distance from the measurement point outside the pit to the diaphragm wall, and D_{max} is the maximum excavation depth of the pit. This convention applies to all subsequent discussions.

In Fig. 9, the model test results aligned well with the measured data. As the normalized distance d/D_{max} increased, the normalized surface settlement δ/δ_{max} initially increased, then decreased, and ultimately approached 0 at a certain distance outside the pit.

4 Settlement analysis

The model tests can only evaluate surface settlement at a fixed point; they cannot continuously measure settlement in the depth direction throughout the structure. Therefore, only the data collected from the designated monitoring points were analyzed. Surface settlement typically occurs in two types, and the triangle-type refers to a settlement pattern observed during foundation pit excavation, characterized by a triangular distribution with the maximum settlement occurring at the edge of the pit. The groove-type describes a settlement profile that gradually decreases from the edge of the pit outward, forming a distribution pattern similar to a groove, and the maximum settlement occurs at a certain distance away from the foundation pit.

4.1 Distribution of surface settlement during dry excavation

Figure 10 illustrates the surface settlement outside the pit for insertion ratios of 0.50, 0.75, 1.00, and 1.25 during dry excavation. When the excavation depth was shallow, the surface settlement outside the pit decreased monotonically with the distance from the diaphragm wall. At greater excavation depths, the surface settlement first increased and then decreased, ultimately approaching 0 beyond a certain distance from the pit.

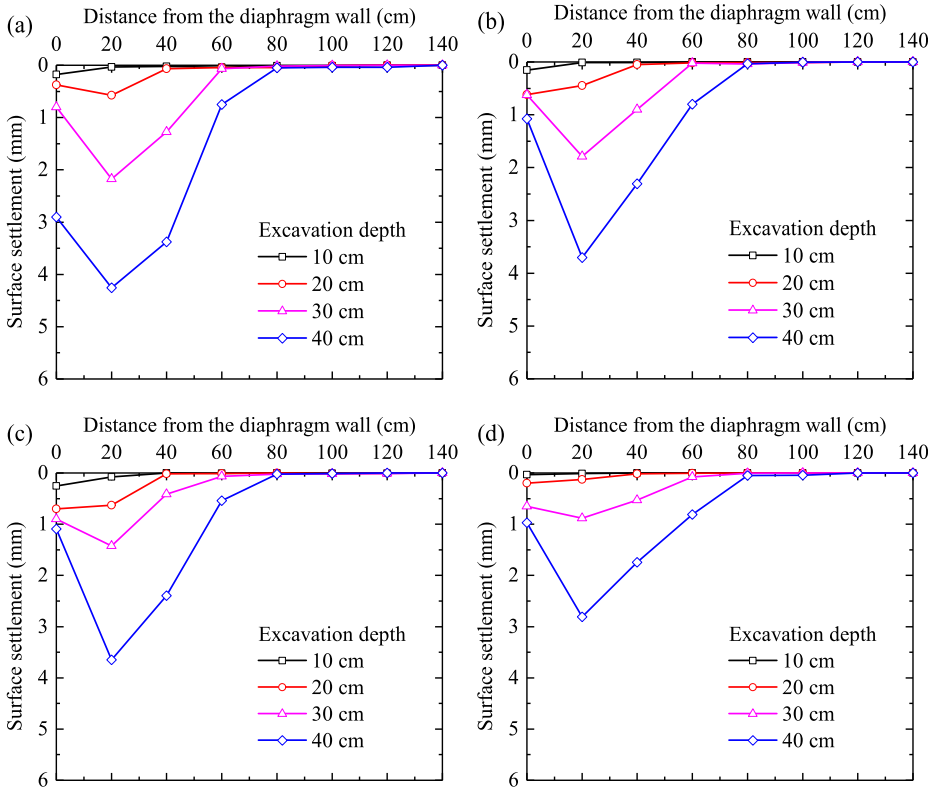

Fig. 10. Distributions of surface settlement outside the pit during dry excavation. (a) $n = 0.50$, (b) $n = 0.75$, (c) $n = 1.00$, and (d) $n = 1.25$.

Taking $n = 1.00$ as an example, at excavation depths of 10 and 20 cm, the maximum surface settlement occurred directly at the diaphragm wall (0.256 and 0.728 mm, respectively). However, at excavation depths of 30 and 40 cm, the maximum settlement occurred 20 cm from the diaphragm wall (1.791 and 3.702 mm, respectively). Thus, as excavation depth increased, the settlement distribution outside the pit shifted from a "triangle" to a "groove" profile. When the excavation depth was shallow, the surface settlement outside the pit primarily resulted from the deformation of the diaphragm wall. At greater depths, the support within the pit restricted further deformation of the diaphragm wall, causing it to bulge laterally.

For dry excavation, the surface settlement outside the pit was affected within 2 times the excavation depth, and the surface settlement decreased to 0 beyond the influence area of excavation. Taking $n = 0.50$ as an example, for excavation depths of 20, 30, and 40 cm, the corresponding

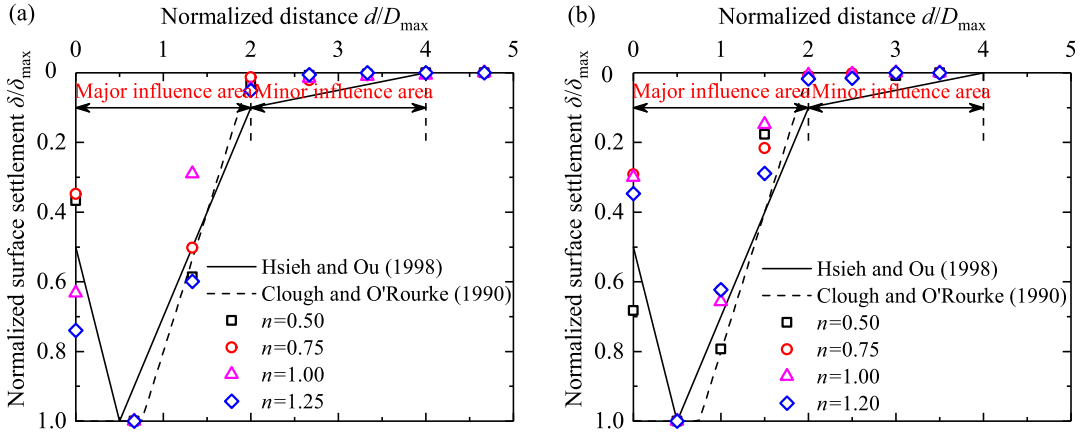

Fig. 11. Comparison of the normalized distributions of surface settlement in dry excavation and empirical estimation curves. (a) $D_{max} = 30$ cm, and (b) $D_{max} = 40$ cm.

distances where surface settlement decreased to 0 were 40, 60, and 80 cm, respectively. This observation aligns with the findings of Clough and O'Rourke (1990).

To analyze the influence area of surface settlement outside the dry excavation pit, two types of distribution curves were referenced: (i) Clough and O'Rourke (1990) introduced an empirical curve for groove-type surface settlement during foundation excavation to estimate surface settlement at various distances behind the wall; and (ii) Hsieh and Ou (1998) proposed corrections and delineated the major and minor settlement influence areas.

Due to the relatively small surface settlement values at excavation depths of 10 and 20 cm, we focused only on the surface settlement data outside the pit at excavation depths of 30 and 40 cm. Figure 11 compares the normalized distributions of surface settlement and the empirical estimation curves for dry excavation at depths of 30 and 40 cm. Using dimensionless parameters allowed us to examine the variation in δ/δ_{max} with d/D_{max}.

The area affected by surface settlement outside the pit during dry excavation aligned more closely with the estimation curve proposed by Clough and O'Rourke (1990) than that proposed by Hsieh and Ou (1998), which decreased to 0 at a distance of twice the excavation depth from the pit. However, near the diaphragm wall, the results aligned much more closely to the surface settlement estimation curve suggested by Hsieh and Ou (1998).

4.2 Surface settlement distribution during dewatering excavation

Figure 12 shows the distributions of surface settlement outside the pit for insertion ratios of 0.50, 0.75, 1.00, and 1.25 during dewatering excavation. When the excavation depth was shallow, the surface settlement outside the pit decreased monotonically with distance from the diaphragm wall. At greater excavation depths, the surface settlement first increased and then decreased. For instance, at $n = 1.00$ and excavation depths of 10 and 20 cm, the maximum surface settlement occurs directly at the diaphragm wall (0.176 and 0.638 mm, respectively). However, at excavation depths of 30 and 40 cm, the maximum settlement occurs 20 cm away from the diaphragm wall (0.5 times the excavation depth), reaching 1.937 and 6.593 mm, respectively. This indicates a shift in the settlement distribution from a "triangle" type to a "groove" type as excavation depth increased. As excavation depth increased, the maximum surface settlement significantly increased compared to under dry excavation conditions. This can be attributed to the effect of groundwater drawdown inside the pit, which affected the groundwater level outside the pit, leading to additional consolidation and settlement of the soil.

Under dewatering excavation conditions, the surface settlement outside the pit was affected beyond 2 times the excavation depth. Taking $n = 0.50$ as an example, a

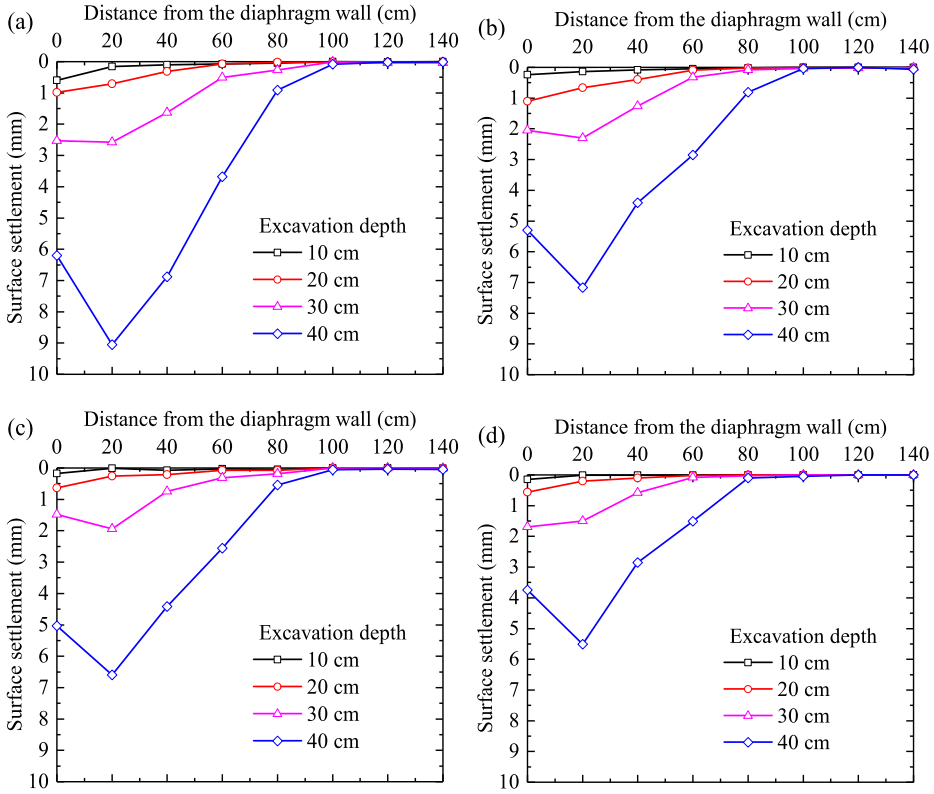

Fig. 12. Distributions of surface settlement outside the pit during dewatering excavation. (a) $n = 0.50$, (b) $n = 0.75$, (c) $n = 1.00$, and (d) $n = 1.25$.

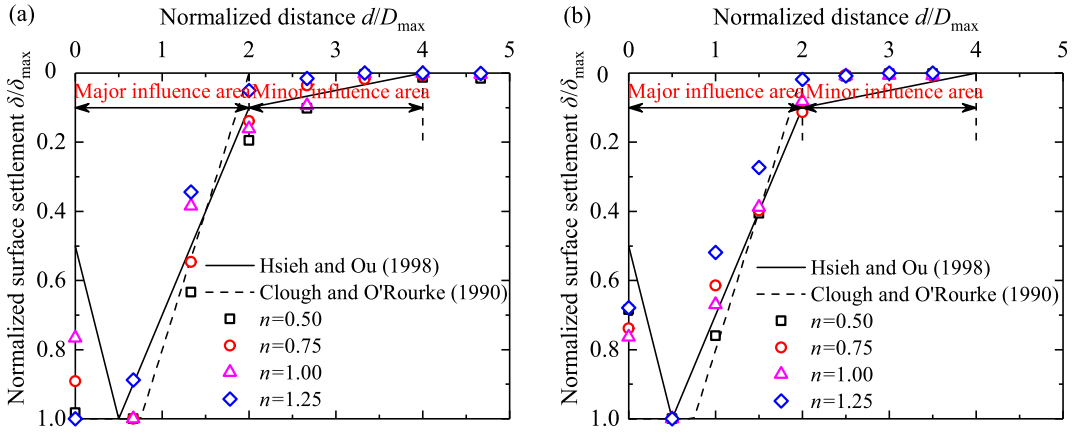

Fig. 13. Distributions of surface settlement outside the pit during dewatering excavation. (a) D_{max} = 30 cm, and (b) D_{max} = 40 cm.

measurable amount of additional settlement occurred outside the pit at distances of 40, 60, and 80 cm (0.311, 0.502, and 0.913 mm, respectively). This indicates that dewatering during excavation enlarged the primary area of settlement influence outside the pit. These findings align with those of Hsieh and Ou (1998), who reported that an inflection point where settlement gradually decreases to 0 appeared at 2 times the excavation depth.

For n = 1.25, the primary influence area of surface settlement outside the pit was confined to 2 times the excavation depth. Thus, as the diaphragm wall insertion ratio increased, the area of surface settlement influence outside the pit tended to decrease. This is because the insertion ratio of the diaphragm wall affected the groundwater seepage field both inside and outside the pit.

The surface settlement outside the pit at excavation depths of 30 and 40 cm was considered in this study. Figure 13 compares the normalized distributions of surface settlement and the empirically estimated curves.

The normalized distributions of surface settlement outside the pit during dewatering excavation are closely aligned with the estimated curves proposed by Hsieh and Ou (1998). Notably, additional settlement was observed at a distance of two times the excavation depth. More than

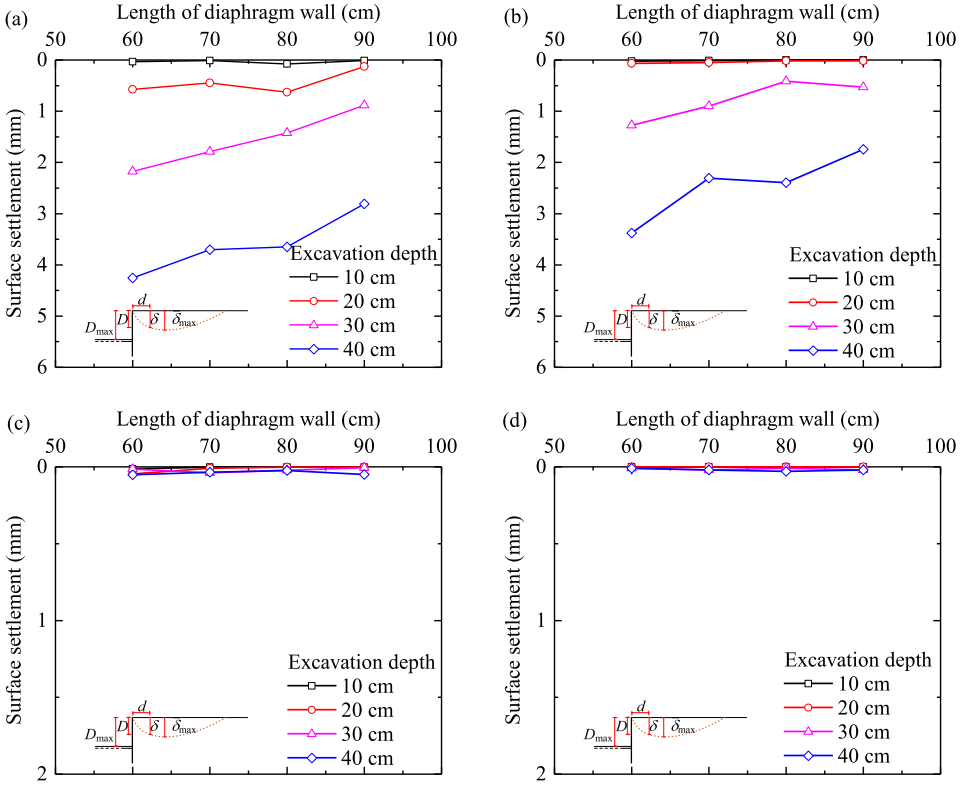

Fig. 14. Surface settlement outside pit during dry excavation over the length of the diaphragm wall. (a) $d = 0.5D_{max}$, (b) $d = D_{max}$, (c) $d = 2D_{max}$, and (d) $d = 2.5D_{max}$.

two times the excavation depth, the normalized surface settlement δ/δ_{max} gradually decreased as the normalized distance d/D_{max} increased, which is consistent with the characteristics of the minor influence area described by Hsieh and Ou (1998).

As shown in Fig. 13, when n increased to 1.25, the influence area of surface settlement outside the pit decreased significantly, and the area of minor influence became almost negligible. Thus, as the buried depth of the diaphragm wall increased, the area of influence of surface settlement caused by dewatering within the pit gradually decreased.

5 Discussion

By analyzing the distribution of surface settlement outside the pit under various conditions, two phenomena emerged that warrant further discussion. First, as the insertion ratio of the diaphragm wall increased, the range of surface settlement during foundation pit dewatering decreased. To clearly define these differences in surface settlement range, it is essential to propose a critical value for the diaphragm wall insertion ratio. Second, regardless of whether the excavation was dry or involved dewatering, the surface settlement outside the pit transitioned from a triangle-type to a groove-type during foundation pit excavation. These two phenomena are crucial for improving the understanding of surface settlement behavior under different excavation scenarios.

5.1 Changes in the extent of the influence of settlement outside the pit

Figure 14 illustrates the relationship between the distribution of surface settlement at different characteristic positions and the insertion ratio of the diaphragm wall during dry excavation. The characteristic positions were defined as $0.5D_{max}$, D_{max}, $2D_{max}$, and $2.5D_{max}$ for an excavation depth of 40 cm ($D_{max} = 40$ cm). At the positions of $0.5D_{max}$ and D_{max}, the surface settlement decreased monotonically with increasing the length of the diaphragm wall. This trend indicates that increasing the insertion ratio effectively confined the development of the major settlement area outside the pit.

At the position of $0.5D_{max}$, when the length of the diaphragm wall increased from 60 to 90 cm, the surface settlement decreased by 34.08% from 4.258 to 2.807 mm. A similar trend was observed at D_{max}, the surface settlement decreased by 48.25% from 3.376 to 1.747 mm. In contrast, at the positions of $2D_{max}$ and $2.5D_{max}$ outside the pit, the surface settlement values were very small; surface settlement remained below 0.050 mm, considerably less than 0.1 times the maximum settlement. This indicated that areas beyond two times the excavation depth were not included in the major area influenced by settlement.

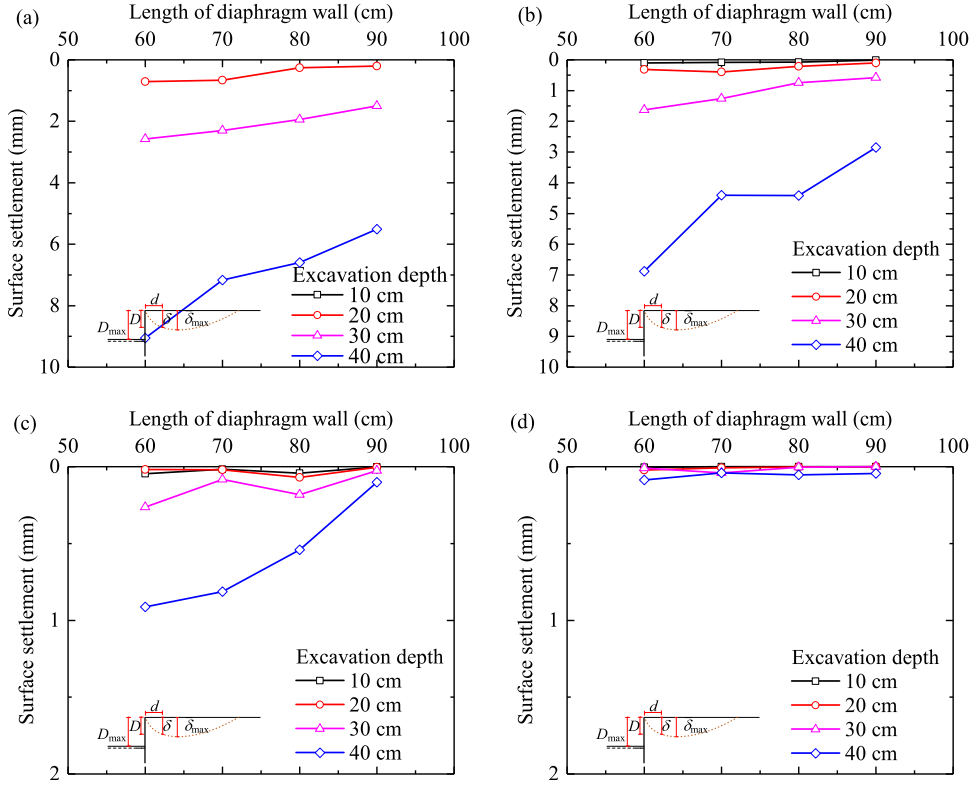

Fig. 15. Surface settlement outside the pit during dewatering excavation over the length of the diaphragm wall. (a) $d = 0.5D_{max}$, (b) $d = D_{max}$, (c) $d = 2D_{max}$, and (d) $d = 2.5D_{max}$.

Figure 15 illustrates the relationship between the distribution of surface settlement at different characteristic positions and the insertion ratio of the diaphragm wall during dewatering excavation. The characteristic positions were defined as $0.5D_{max}$, D_{max}, $2D_{max}$, and $2.5D_{max}$ for an excavation depth of 40 cm ($D_{max} = 40$ cm). At the positions of $0.5D_{max}$, D_{max}, and $2D_{max}$, the surface settlement outside the pit decreased monotonically with increasing the length of the diaphragm wall. Thus, increasing the buried depth of the diaphragm wall effectively confined the development of surface settlement in the major area of settlement influence outside the pit.

At the position of $0.5D_{max}$, when the length of the diaphragm wall increased from 60 to 90 cm, the surface settlement decreased by 39.20% from 9.057 to 5.507 mm. At the D_{max} position, the surface settlement decreased by 58.48% from 6.879 to 2.856 mm. At $2D_{max}$, the surface settlement decreased by 88.83% from 0.913 to 0.102 mm. At $2.5D_{max}$, the surface settlement values were very small; surface settlement remained below 0.100 mm, much less than 0.1 times the maximum settlement. Thus, when the buried depth of the diaphragm wall was relatively shallow ($n < 1.25$), the area beyond two to four times the excavation depth represented a minor area of settlement influence, consistent with the findings of Hsieh and Ou (1998). Conversely, when buried depth was relatively deep ($n \geq 1.25$), the area beyond two times the excavation depth was classified as a minor area of settlement influence, aligning with the results of Clough and O'Rourke (1990).

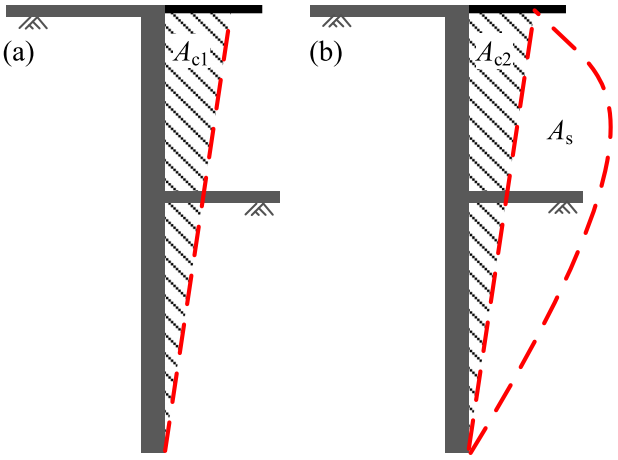

Fig. 16. Schematic diagram of the areas of the cantilever and deep inward components of the diaphragm wall. (a) First excavation step, and (b) current excavation step.

5.2 Changes in the pattern of settlement outside the pit

Clough and O'Rourke (1990) studied the evolution of surface settlement patterns outside the pit and introduced two area parameters: A_s, which represents the area of the deep inward part of the convex deformation of the diaphragm wall; and A_c, which refers to the cantilever part of the diaphragm wall. These parameters can be calculated as follows:

$$A_{c1} = \max(A_{c1}, A_{c2}), \tag{2}$$

where A_{c1} represents the cantilever lateral displacement value of the diaphragm wall caused by the first step of excavation, while A_{c2} refers to the cantilever part of the total lateral movement of the diaphragm wall resulting from the current excavation.

The areas associated with the cantilever and deep inward parts of the lateral movement of the diaphragm wall are illustrated in Fig. 16.

To establish the relationship between the type of settlement pattern and the lateral displacement shape of the diaphragm wall, Hsieh and Ou (1998) examined nine typical engineering cases. They proposed that groove-type settlement occurs when $A_s \geq 1.6A_c$, whereas triangle-type settlement occurs under other conditions.

For $n = 0.75$ (corresponding to a depth of 70 cm), the deflection of the diaphragm wall was calculated using the monitoring data from strain gauges attached along the centerline of the diaphragm wall. With the end of the diaphragm wall serving as the base point, the strain gauge monitoring data was converted to obtain the change in wall deflection with depth.

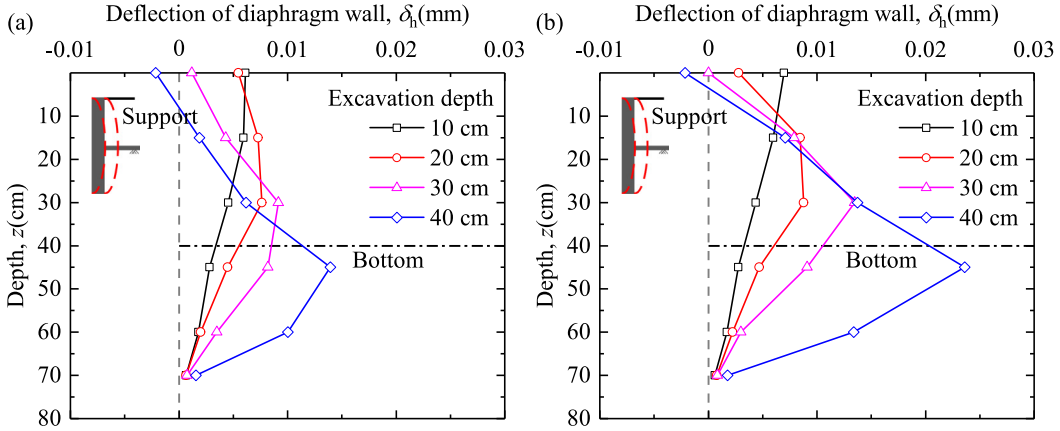

Fig. 17. Distribution of diaphragm wall deflection over excavation depth. (a) Dry excavation, and (b) dewatering excavation.

Table 3
Calculated area parameters.

Conditions	Excavation depth (cm)	A_s (mm^2)	A_c (mm^2)	1.6A_c (mm^2)
Dry excavation	10	0.00	2.10	3.36
	20	1.72	2.10	3.36
	30	3.42	2.10	3.36
	40	4.89	2.10	3.36
Dewatering excavation	10	0.00	2.45	3.92
	20	2.62	2.45	3.92
	30	4.73	2.45	3.92
	40	8.26	2.45	3.92

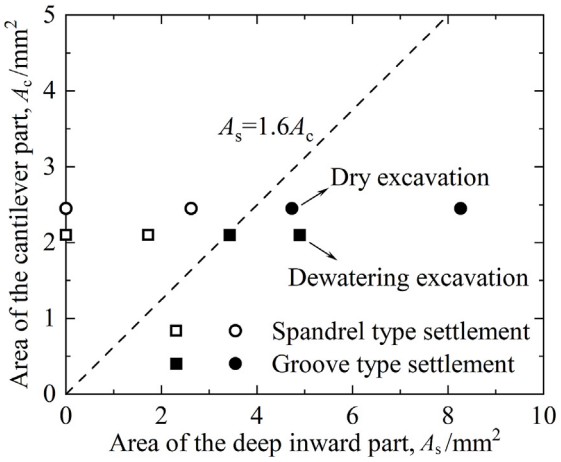

Fig. 18. Relationship between the area of the cantilever component and the area of the deep inward component of the diaphragm wall.

Figure 17 illustrates the distribution of lateral displacement along the depth of the diaphragm wall during both dewatering excavation and dry excavation. Here, δ_h represents the deflection of the diaphragm wall; positive values indicate deflection toward the inside of the pit, whereas negative values indicate outward deflection. The trend in deflection for the diaphragm wall was similar during both excavation methods, with the deflection value increasing with increasing excavation depth (i.e., an "inner convex" type of deformation). This behavior can be attributed to the reinforced concrete support, which limited the deformation at the top of the diaphragm wall. As excavation depth increased, the maximum deflection of the diaphragm wall gradually shifted downward and consistently appeared near the bottom of the excavation depth. Comparing Fig. 17(a) and (b) reveals a notable difference: the flexural deformation values of the diaphragm wall during dewatering excavation were larger than those observed during dry excavation. For instance, at an excavation depth of 40 cm, the maximum lateral displacement of the diaphragm wall during dewatering excavation reached 0.024 mm, while that during dry excavation was only 0.014 mm.

The values of A_s and A_c after each excavation step were calculated; these steps are summarized in Table 3. Figure 18 is based on the data presented in Table 3. According to Hsieh and Ou (1998), for $n = 0.75$, both dewatering and dry excavation resulted in triangle-type settlement at excavation depths of 10 and 20 cm. However, at excavation depths of 30 and 40 cm, the surface settlement type shifted to groove type. This finding is consistent with the experimental results presented in Section 4.

This section thoroughly investigated the relationship between surface settlement and the lateral displacement of the diaphragm wall by controlling the insertion depth of the diaphragm wall, we established the relationship between surface settlement and lateral displacement of the diaphragm wall. The discussion can serve as a reference for resilient underground design.

6 Conclusions

A series of laboratory-scale experiments was conducted under both dry excavation and dewatering excavation conditions. The surface settlement values, areas of settlement influence, and settlement patterns outside the pit were analyzed under various excavation conditions and different diaphragm wall insertion ratios. The key conclusions are summarized as follows.

(1) The combined effect of dewatering and excavation significantly affected surface settlement. The interaction between dewatering and excavation increased the surface settlement values outside the pit and expanded the area of settlement influence.
(2) The diaphragm wall insertion ratio significantly affected surface settlement. As the insertion ratio increased, the surface settlement gradually decreased, and the area affected by surface settlement became smaller. Specifically, when the insertion ratio increased from 0.50 to 1.25, the surface settlement outside the pit decreased from 39.20% to 88.83%.
(3) Under dewatering conditions, the accuracy of different settlement estimation curves depended on the diaphragm wall insertion ratio. The area beyond two times the excavation depth represented a minor area of settlement influence for $n < 1.25$, whereas the area beyond two times the excavation depth wasn't classified as a minor area of settlement influence for $n \geq 1.25$.

(4) The surface settlement pattern could be effectively estimated using the diaphragm wall deformation disassembly method. As excavation depth increased, the surface settlement pattern outside the pit transitioned from triangle type to groove type. Groove-type settlement occurred when the A_s value of the deep inward part of the convex deformation in the diaphragm wall was at least $1.6A_c$.

Data availability

The data that support the findings of this study are available from the corresponding author upon reasonable request.

CRediT authorship contribution statement

Kai-Fang Yang: Writing – original draft, Validation, Methodology, Investigation, Formal analysis, Data curation, Conceptualization. **Min-Liang Chi:** Writing – original draft, Validation, Methodology, Investigation, Formal analysis, Data curation. **Chang-Jie Xu:** Writing – review & editing, Supervision, Resources, Project administration, Formal analysis, Conceptualization. **Chao-Feng Zeng:** Writing – review & editing, Methodology, Investigation, Data curation. **Lu-Ju Liang:** Writing – review & editing, Validation, Methodology, Investigation. **Zhi Ding:** Writing – review & editing, Methodology, Formal analysis, Data curation. **Ya-Shi Qiu:** Writing – original draft, Methodology, Investigation, Formal analysis, Data curation.

Declaration of competing interest

The authors declare that they have no known competing financial interests or personal relationships that could have appeared to influence the work reported in this paper.

Acknowledgement

This work was supported by the National Key Research and Development Program of China (Grant No. 2023YFC3009400) and the National Natural Science Foundation of China (Grant Nos. 52508413, 52238009, and U1934208). Finally, we deeply appreciate the warm and efficient work of editors and reviewers.

References

Abbas, Q., Yoon, J., & Lee, J. (2023). Characterization of wall deflection and ground settlement for irregular-shaped excavations with changes in corner configuration. *International Journal of Geomechanics*, *23*(1), 04022258.

ASTM (2011). *ASTM D2487-11: Standard practice for classification of soils for engineering purpose*. PA, USA: ASTM International.

Chen, H. H., Li, J. P., & Li, L. (2018). Performance of a zoned excavation by bottom-up technique in Shanghai soft soils. *Journal of Geotechnical and Geoenvironmental Engineering*, *144*(11), 05018003.

Clough, G. W., & O'Rourke, T. D. (1990). Construction induced movements of in-situ wall. In *Proceedings of Specialty Conference on Design and Performance of Earth Retaining Structures* (pp. 439–470). New York.

Cui, J. F., Yang, Z. K., & Azzam, R. (2023). Field measurement and numerical study on the effects of under-excavation and over-excavation on ultra-deep foundation pit in coastal area. *Journal of Marine Science and Engineering*, *11*(1), 219.

Ding, H. B., Wan, Q. W., Xu, C. J., Fan, X. Z., & Tong, L. H. (2024). Semianalytical method for controlling the deformation of retaining structures subjected to asymmetrical loads. *International Journal of Geomechanics*, *24*(4), 04024031.

Dong, J. C., Bai, Q., Zhao, W., & Wang, B. D. (2023). Test study on the influence of foundation pit excavation on the surface settlement of sandy soil natural foundation of adjacent buildings. *Buildings*, *13*(5), 1293.

Fan, X. Z., Xu, C. J., Liang, L. J., Chen, Q. Z., & Deng, J. L. (2021). Analytical solution for displacement-dependent passive earth pressure on rigid walls with various wall movements in cohesionless soil. *Computers and Geotechnics*, *140*, 104470.

Fan, X. Z., Xu, C. J., Liang, L. J., Yang, K. F., Chen, Q. Z., Feng, G. H., & Zhang, J. Z. (2024). Experimental and numerical study of braced retaining piles with asymmetrical excavation. *International Journal of Civil Engineering*, *22*(8), 1339–1356.

Ge, C. H., Yang, M., Li, P. F., Zhang, M. J., & Zhang, Z. H. (2024). Performance and environmental impacts of deep foundation excavation in soft soils: A field and modeling-based case study in Nanjing, China. *Underground Space*, *18*, 218–238.

Guan, L. X., Wang, P., Ding, H. B., Qin, J. L., Xu, C. J., & Feng, G. H. (2024). Analysis of settlement of an existing tunnel subjected to undercrossing tunneling based on the modified vlasov model. *International Journal of Geomechanics*, *24*(3), 04023300.

Hsi, J. P., & Small, J. C. (1992). Ground settlements and drawdown of the water table around an excavation. *Canadian Geotechnical Journal*, *29*(5), 740–756.

Hsieh, P. G., & Ou, C. Y. (1998). Shape of ground surface settlement profiles caused by excavation. *Canadian Geotechnical Journal*, *35*(6), 1004–1017.

Li, H., Huang, M. S., Yu, J., Li, Y. H., & Guo, Y. C. (2024). Three-dimensional solution for braced excavation-induced ground settlement. *Computers and Geotechnics*, *172*, 106460.

Li, J., Xia, X. H., Li, M. G., Chen, J. J., & Zhan, H. B. (2020a). Nonlinear drainage model of viscoelastic aquitards considering non-darcian flow. *Journal of Hydrology*, *587*, 124988.

Li, M. G., Chen, J. J., Xia, X. H., Zhang, Y. Q., & Wang, D. F. (2020b). Statistical and hydro-mechanical coupling analyses on groundwater drawdown and soil deformation caused by dewatering in a multi-aquifer-aquitard system. *Journal of Hydrology*, *589*, 125365.

Li, Z., Zhao, G. F., Deng, X. F., Zhu, J. B., & Zhang, Q. B. (2022). Further development of distinct lattice spring model for stability and collapse analysis of deep foundation pit excavation. *Computers and Geotechnics*, *144*, 104619.

Luo, G. Y., Qiu, J. S., Cao, H., & Pan, H. (2018). Simplified method for calculating inflow into a deep excavation with consideration of the effects of cutoff walls. *Hydrogeology Journal*, *26*(8), 2853–2865.

Ministry of Water Resources of the People's Republic of China (2007). GB/T 50145—2007: Standard for Engineering Classification of Soil. Beijing, China, China Planning Press (in Chinese).

Ou, C. Y., Hsieh, P. G., & Chiou, D. C. (1993). Characteristics of ground surface settlement during excavation. *Canadian Geotechnical Journal*, *30*(5), 758–767.

Park, Y. J., Hwang, H. T., Suzuki, S., Saegusa, H., Nojiri, K., Tanaka, T., Bruines, P., Abumi, K., Morita, Y., & Illman, W. A. (2020). Improving precision in regional scale numerical simulations of groundwater flow into underground openings. *Engineering Geology*, *274*, 105727.

Ping, S. F., Wang, F. G., Wang, D. H., Li, S. W., Yuan, Y. L., Wu, M. J., Pan, H. L., & Cao, Y. Q. (2024). Optimization of a deep foundation pit dewatering scheme in gypsum-bearing strata. *Environmental Earth Sciences*, *83*(1), 8.

Pujades, E., & Jurado, A. (2021). Groundwater-related aspects during the development of deep excavations below the water table: A short review. *Underground Space*, *6*(1), 35–45.

Pujades-Garnes, E., Badiella, G., Jurado, A., Carrera, J., & Vazquez-Suñe, E. (2024). An approach for the design of dewatering systems: The case of an excavation for the construction of the assembly shaft of a tunnel boring machine. *Bulletin of Engineering Geology and the Environment*, *83*(7), 296.

Serrano-Juan, A., Pujades, E., Vázquez-Suñè, E., Crosetto, M., & Cuevas-González, M. (2017). Leveling vs. InSAR in urban underground construction monitoring: Pros and cons. Case of la sagrera railway station (Barcelona, Spain). *Engineering Geology*, *218*, 1–11.

Serrano-Juan, A., Pujades, E., Vázquez-Suñé, E., Velasco, V., Criollo, R., & Jurado, A. (2018). Integration of groundwater by-pass facilities in the bottom slab design for large underground structures. *Tunnelling and Underground Space Technology*, *71*, 231–243.

Tan, Y., Lu, Y., & Wang, D. L. (2018). Deep excavation of the gate of the orient in Suzhou stiff clay: Composite earth-retaining systems and dewatering plans. *Journal of Geotechnical and Geoenvironmental Engineering*, *144*(3), 05017009.

Tang, C., He, S. Y., & Zhou, W. H. (2024). An efficient physics-guided Bayesian framework for predicting ground settlement profile during excavations in clay. *Journal of Rock Mechanics and Geotechnical Engineering*, *16*(4), 1411–1424.

Wang, D. Q., Ye, S. H., & Xin, L. L. (2023). Study on the analysis of pile foundation deformation and control methods during the excavation of deep and thick sludge pits. *Water*, *15*(17), 3121.

Wang, J. X., Long, Y. X., Gao, F., Wang, H. M., Shi, Y. J., Yang, T. L., Liu, X. T., Huang, X. L., & Xu, N. (2022). Transparent soil test evaluation of vertical–horizontal mixed curtain during dewatering. *Acta Geotechnica*, *17*, 3293–3313.

Wang, X. W., Yang, T. L., Xu, Y. S., & Shen, S. L. (2019). Evaluation of optimized depth of waterproof curtain to mitigate negative impacts during dewatering. *Journal of Hydrology*, *577*, 123969.

Wu, Y. X., Shen, S. L., Lyu, H. M., & Zhou, A. N. (2020). Analyses of leakage effect of waterproof curtain during excavation dewatering. *Journal of Hydrology*, *583*, 124582.

Xu, C. J., Yang, K. F., Fan, X. Z., Ge, J. J., & Jin, L. (2021). Numerical investigation on instability of buildings caused by adjacent deep excavation. *Journal of Performance of Constructed Facilities*, *35*(5), 04021040.

Xu, Y. S., Yan, X. X., Shen, S. L., & Zhou, A. N. (2019). Experimental investigation on the blocking of groundwater seepage from a waterproof curtain during pumped dewatering in an excavation. *Hydrogeology Journal*, *27*(7), 2659–2672.

Xue, X. L., Sun, H. Y., Zeng, C. F., Chen, H. B., Zheng, G., Xu, C. J., & Han, L. (2024). Why pile-supported building settled continuously after water level was stabilized during dewatering: Clues from interaction between pile and multi aquifers. *Journal of Hydrology*, *638*, 131539.

Yang, K. F., Xu, C. J., Chi, M. L., & Wang, P. (2022). Analytical analysis of the groundwater drawdown difference induced by foundation pit dewatering with a suspended waterproof curtain. *Applied Sciences*, *12*(20), 10301.

Yang, Y. B., Chen, C. Y., Liu, C., Huang, L. T., Chen, W., Lin, N. Y., Cui, J., & Xie, W. D. (2023). Performance of a deep excavation and the influence on adjacent piles: A case history in karst region covered by clay and sand. *Underground Space*, *8*, 45–60.

Zeng, C. F., Song, W. W., Xue, X. L., Li, M. K., Bai, N., & Mei, G. X. (2021). Construction dewatering in a metro station incorporating buttress retaining wall to limit ground settlement: Insights from experimental modelling. *Tunnelling and Underground Space Technology*, *116*, 104124.

Zeng, C. F., Wang, S., Xue, X. L., Zheng, G., & Mei, G. X. (2022). Characteristics of ground settlement due to combined actions of groundwater drawdown and enclosure wall movement. *Acta Geotechnica*, *17*(9), 4095–4112.

Zeng, C. F., Zhang, Z. H., Gao, W. H., Cai, G., Zhu, L., Chen, H. B., Xue, X. L., & He, J. Q. (2023). Barrier effects of surrounding group piles on deformation of foundation pits induced by dewatering. *Chinese Journal of Geotechnical Engineering*, *45*(11), 2378–2386 (in Chinese).

Zeng, C. F., Powrie, W., Chen, H. B., Wang, S., Diao, Y., & Xue, X. L. (2024). Ground behavior due to dewatering inside a foundation pit considering the barrier effect of preexisting Building Piles on Aquifer Flow. *Journal of Geotechnical and Geoenvironmental Engineering*, *150*(6), 05024004.

Zhang, W. G., Goh, A. T. C., Goh, K. H., Chew, O. Y. S., Zhou, D., & Zhang, R. H. (2018a). Performance of braced excavation in residual soil with groundwater drawdown. *Underground Space*, *3*(2), 150–165.

Zhang, W. S., Yuan, Y., Long, M., Yao, R. H., Jia, L., & Liu, M. (2024). Prediction of surface settlement around subway foundation pits based on spatiotemporal characteristics and deep learning models. *Computers and Geotechnics*, *168*, 106149.

Zhang, Y. Q., Wang, J. H., Chen, J. J., & Li, M. G. (2017). Numerical study on the responses of groundwater and strata to pumping and recharge in a deep confined aquifer. *Journal of Hydrology*, *548*, 342–352.

Zhang, Y. Q., Wang, J. H., & Li, M. G. (2018b). Effect of dewatering in a confined aquifer on ground settlement in deep excavations. *International Journal of Geomechanics*, *18*(10), 04018120.

Zheng, G., Li, Q. H., Cheng, X. S., Ha, D., Shi, J. C., Shi, X. R., & Lei, Y. W. (2024). Diaphragm wall deformation and ground settlement caused by dewatering before excavation in strata with leaky aquifers. *Géotechnique*, *74*(1), 1–17.